8-2018

Testing and Development of Pre-Stressed CFRP Retrofit Strategies for Controlling Fatigue Cracking in Steel Waterway Lock Gate Structures

Maggie Langston
University of Arkansas, Fayetteville

Testing and Development of Pre-Stressed CFRP Retrofit Strategies for Controlling Fatigue Cracking in Steel Waterway Lock Gate Structures

A thesis submitted in partial fulfillment
of the requirements for the degree of
Master of Science in Civil Engineering

by

Maggie Langston
University of Arkansas
Bachelor of Science in Civil Engineering, 2017

August 2018
University of Arkansas

This thesis is approved for recommendation to the Graduate Council.

Gary Prinz, PhD
Thesis Director

Cameron Murray, PhD
Committee Member

Micah Hale, PhD
Committee Member

Abstract

Steel waterway lock gates across the national inland waterway transportation network are reaching and exceeding their intended service life, often experiencing component failures that lead to service interruptions. Unscheduled maintenance and repair of lock gates can be expensive and cause economic ripples throughout the entire inland waterway network. These lock gate component failures are often caused by fatigue cracking from repeated loading during operation. This thesis develops and tests a prestressed carbon fiber reinforced polymer (CFRP) fatigue retrofit for controlling fatigue demands within lock gate components. The study expands upon a recent analytical work by Lozano (2017) by experimentally investigating prestressing strategies, bonding mechanisms, prestress creep/relaxation performance, and large-scale experimental fatigue testing. A total of seven large-scale cyclic tests were conducted on lock gate components (with and without applied retrofits) to gauge the effectiveness of the developed prestressing strategies. All gate specimens tested were artificially notched to create a local stress concentration and worsened fatigue condition. Results indicate that the addition of the prestressed CFRP retrofit increases the fatigue life of the retrofitted gate component despite the prestress loss due to epoxy adhesive debonding following rapid cyclic loading. The retrofitted specimen experienced a fatigue life increase of nearly 3 times over the un-retrofitted specimen. Additionally, load shedding into the CFRP, even without significant prestress applied, contributes to a reduction in the component notch stress. The applied CFRP clamping force is able to provide enough force transfer to the CFRP to reduce the notch local stresses.

Acknowledgements

This thesis is part of a research project funded by the Maritime Transportation Research and Education Center (MarTREC) and the U.S. Department of Transportation under Grant Award Number DTRT13-G-UTC50. Material support was given by MarTREC and laboratory staff at the Engineering Research Center (ENRC) including Mark Kuss and David Peachee as well as assistance from Dr. Guillermo Riveros from the U.S. Army Corps of Engineers. The authors also acknowledge in-kind support by W&W|AFCO Steel who provided the steel and fabricated the large-scale experimental specimens. This research was conducted in the Steel Structures Research Laboratory (SSRL) at the University of Arkansas with student help of Christine Lozano and Diego Real.

Disclaimer

The contents of this report reflect the views of the authors, who are responsible for the facts and the accuracy of the information presented herein. This document is disseminated under the sponsorship of the U.S. Department of Transportation's University Transportation Centers Program, in the interest of information exchange. The U.S. Government assumes no liability for the contents or use thereof.

Table of Contents

List of Figures

List of Tables

1. Introduction

The current average age of existing waterway lock gates within the US waterway transportation network is 67 years [1]. Several existing gates have even exceeded 100 years of service, and are still in operation [1]. Given that the majority of these existing lock gates were designed for an expected service life of 50-years, concern over infrastructure reliability and increased unscheduled service interruptions is growing. In both 2013 and 2017 the American Society of Civil Engineers (ASCE) gave the inland waterway infrastructure a "D" grade based on its age and because nearly 49% of all vessels experienced infrastructure-induced delays [2, 3]. In the ASCE scale, a "D" grade indicates that the infrastructure is in "poor to fair condition" with a "strong risk of failure" [4].

Unscheduled maintenance and repair of lock gates can be expensive and cause economic ripples throughout the entire inland waterway network. As an example, the 2002 upstream lock gate failure on the John Day Lock resulted in eight months of required repairs [5]. A gate deterioration failure within the Greenup Lock in 2003 resulted in an estimated $14 million in losses to barge companies from lost operating costs [6]. The McApline Lock in 2004 is another example, with failure of critical structural members causing over 1,440 hours of tow delays even with a closure notice of 2 months [7]. Failure of the downstream gate on the Dalles Lock in 2009 resulted in two transportation companies temporarily laying off half of their workers [8]. The United States Army Corps of Engineers (USACE) states that waterway lock gates are the "most immediate critical infrastructure component" because of rapid degradation [9].

Lock gate component failures are often caused by fatigue cracking from repeated loading during operation. Fatigue cracking often occurs under service-type loading due to repeated cyclic stresses that are often far below those required for monotonic fracture. The resulting fatigue life

of a component subjected to cyclic loading is dependent on two main loading parameters, 1) the applied stress cycle range and 2) the mean value of the applied stress range (see Figure 1). Typically, higher applied stress ranges and higher mean stresses result in a lower fatigue life.

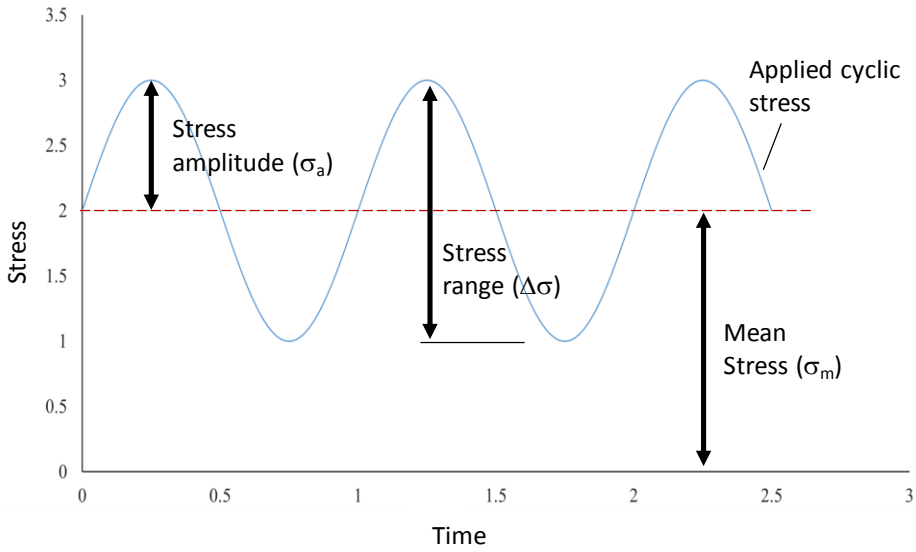

Figure 1. Basic cyclic loading parameters affecting fatigue life of a component.

Many fatigue retrofit methods exist to extend the fatigue life of structural components, with most aiming to lower the applied stress range to reduce fatigue demands. Welding, hole-drilling, plating, and post-tensioning are all common methods of reducing stresses and can be found in the Manual for Repair and Retrofit of Fatigue Cracking in Steel Bridges [10]. Note that weld surface treatments are often applied before fatigue crack initiation to improve the existing weld geometry and eliminate weld-induced tensile residual stresses that translate to high mean stress values [10], while hole-drilling is performed after crack initiation to reduce crack-tip stresses [10]. Adding additional material (welding or bolting plates) near fatigue critical regions is used to reduce the locally applied stress range while post-tensioning retrofits apply local compressive stresses to reduce the applied mean stress [10].

To allow for controlled modification of component stress states, post-tensioning retrofit methods using high-strength fiber reinforced polymer materials were chosen for this study. Since the 2000s, fiber reinforced polymer (FRP) has been tested as a potential retrofitting material due a high strength-to-weight ratio, high corrosion-resistance, and excellent fatigue performance [11]. Carbon FRP (CFRP) can also have a higher elastic modulus than steel (15,900-84,000 ksi) [11]. Research has proven CFRP to be an effective and efficient retrofitting material in the form of bars, patches, and strips for both steel and concrete [12-17]. As an example, Tajsten 2009 showed that prestressed CFRP strips were capable of providing infinite fatigue life to steel plates and that non-prestressed CFRP strips could increase the plate fatigue life by up to 3.74 times [18]. Because of these advantages, prestressed CFRP strips can be bonded to the structure using special adhesives or un-bonded to the structure using anchorage systems.

Un-bonded prestressed CFRP systems have many advantages over traditional bonded CFRP which uses adhesives. Un-bonded systems do not permanently alter the original geometry of the structure and can be applied to a broader range of structures such as riveted bridges or historic landmarks. Additionally, according to Ghafoori 2015 and Lenwari 2006, un-bonded CFRP systems require less time to install (requiring less surface preparation) and reduce de-bonding failures that are often encountered with bonded CFRP retrofits [19, 20]. Unbonded prestressed CFRP applications are chosen for this investigation.

Recent analytical and experimental studies have investigated the effectiveness of prestressed CFRP retrofit methods on fatigue crack mitigation. Analytical research studies by Colombi 2003 and Kianmofrad 2017 showed a reduction in crack tip stress and the insignificance of CFRP geometry when applying a prestressed CFRP retrofit [21, 22]. Mohee 2017 used FEM to develop effective anchorage systems for prestressed CFRP strips and tested them under static

loading [23]. Hong 2017 and Ye 2018 were successful in using un-bonded prestressed CFRP strips to strengthen large-scale concrete and notched steel beams, respectively, with a bolted anchorage system under 3-point bending [24, 25]. Li 2018 used bonded prestressed CFRP strips to strengthen large-scale notched steel beams with an adhesive and bolting anchorage system under 4-point bending [26]. Ghafoori 2015 and 2016 used un-bonded prestressed CFRP strips to strengthen large-scale steel bridge beams with a friction anchorage system under 4-point bending [27, 28]. The goal of this research was to design an un-bonded prestressed CFRP strip retrofit to mitigate fatigue cracking in critical lock gate details.

2. Analytical Fatigue Investigation of the Greenup Lock and Dam by Lozano (2017)

In a recent work by Lozano (2017) [29], an existing lock gate and retrofit were modeled using ABAQUS to identify critical fatigue regions and investigate the effect of prestressed retrofits on component fatigue susceptibility. This section summarizes the study performed by [29], highlighting the fatigue analysis results and suggested prestress levels to achieve an infinite fatigue life within the critical gate region. The lock gate modeled in [29] was the Greenup Lock and Dam on the Ohio River.

In the analytical investigation by [29], twenty-four sections of high stress were identified using the Von Mises stress contours, see Figure 2. Miner's rule (explained later) was then applied to these sections and the highest amount of damage during one lockage cycle was determined to be a cruciform section located on the centerline near the bottom of the downstream side of the gate, see Figure 2(b) and (c). The critical fatigue region, Section F13 in Figure 2, has the smallest cross-sectional area near the point of highest hydrostatic pressure compared to other identified sections. The critical fatigue region was further verified by field observations conducted by the USACE.

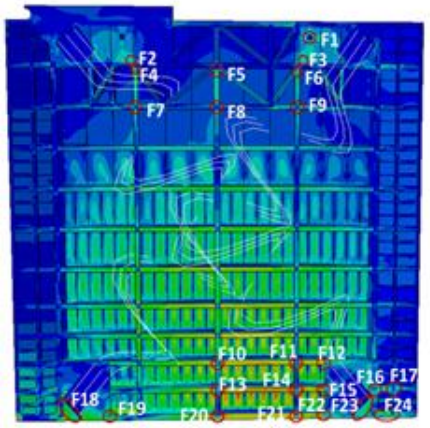

(a)

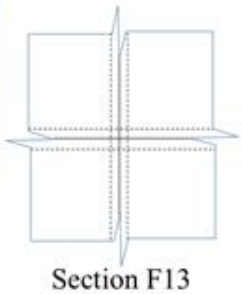

Section F13
Connection Detail

(b)

Location	Δσ (ksi)	Δf (ksi)	Total Damage
Section F7	5.945	4.5	1.910E-07
Section F9	7.093	4.5	3.244E-07
Section F10	22.732	4.5	1.068E-05
Section F11	22.52	4.5	1.038E-05
Section F12	21.584	4.5	9.141E-06
Section F13	23.444	4.5	1.171E-05
Section F14	23.301	4.5	1.150E-05
Section F15	22.022	4.5	9.709E-06
Section F16	9.807	4.5	8.574E-07
Section F17	9.807	4.5	8.574E-07
Section F20	22.411	4.5	1.023E-05
Section F21	21.916	4.5	9.570E-06
Section F22	19.854	4.5	7.114E-06
Section Inside 1	12.534	7	8.950E-07
Section Inside 2	10.37	7	5.069E-07

(c)

Figure 2. FEM stress contours for Greenup Lock gate and critical fatigue detail [29]

In [29], the stress changes to section F13 due to various retrofit prestress forces were analyzed using two methods: 1) a local stress approach using constant life diagrams, and 2) a nominal stress approach using empirical fatigue detail categories found in the AASHTO LRFD Bridge Specification [30]. For clarity in understanding the approach taken by [29], which is also used in this study, the two fatigue evaluation approaches are summarized briefly below.

2.1. *The Local Stress Constant Life Diagram Approach*

In the constant life diagram approach, the fatigue endurance limit (the stress threshold below which no fatigue damage is expected) is based on the ultimate strength of the material and the effects of material surface conditions, size, loading, temperature, reliability, and miscellaneous environmental factors. While many constant life diagrams exist for evaluating fatigue thresholds, [29] chose a modified Goodman criterion because it applies to mild steel materials and accounts for yielding as a failure mode. The Goodman constant life diagram is shown in Figure 3 and presents the infinite and finite fatigue regions for a given material. The fatigue threshold based on the Goodman criterion can be calculated using Equation 1. In Equation 1, σ_a, σ_m, S_e, S_{ult} and n are alternating stress, mean stress, endurance limit stress, ultimate limit stress and a factor of safety

respectively. In Figure 3, combinations of mean stress and stress amplitude from measurements or finite element simulations can be plotted and determined to be in either finite or infinite fatigue life regions.

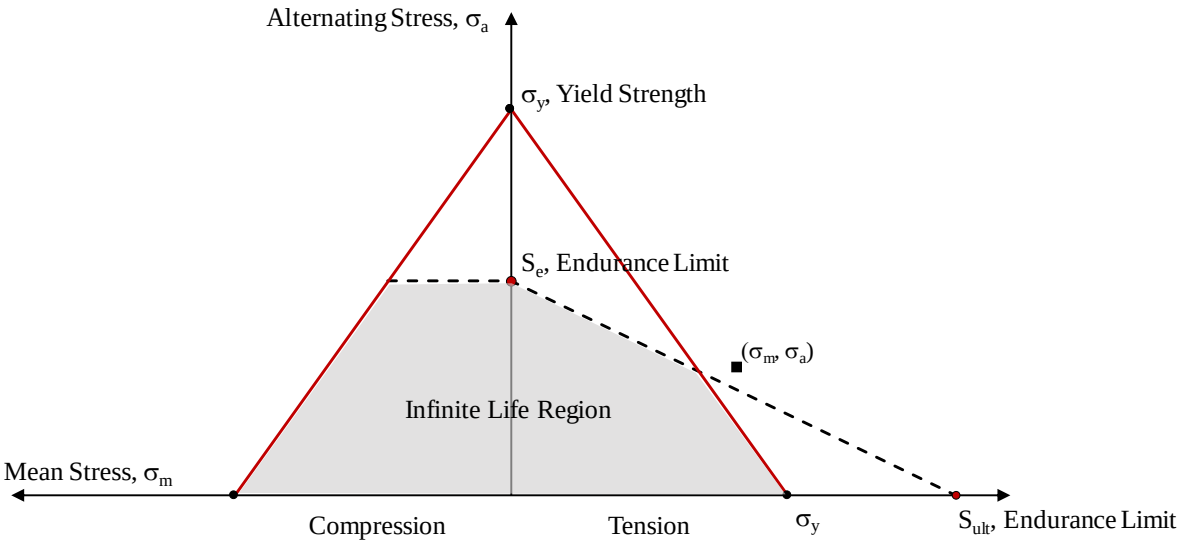

Figure 3. Constant life diagram using the modified Goodman criteria for smooth specimens

$$\frac{\sigma_a}{S_e} + \frac{\sigma_m}{S_{ult}} = \frac{1}{n} \qquad \text{(Equation 1)}$$

2.2. *The AASHTO Nominal Stress Approach*

In the nominal stress approach also taken by [29], the fatigue threshold is based on a selected detail category that considers geometry, loading direction, and connection type (including weld detailing). Damage due to fatigue occurs when the applied stress range is above this fatigue threshold and can be calculated from provided stress-vs-number of cycles to failure (S-N) curves and accumulated using Miner's Rule. Miner's Rule is a linear damage accumulation model in which total damage, D, is equal to the summation of individual damaging constant amplitude cycles, see Equation 2. Using the nominal stress approach such as that provided in AASHTO, an estimated number of cycles to failure can be calculated using empirical S-N curves where A is provided from the detail category, see Equation 3.

$$D = \Sigma D_i = \Sigma \frac{n_i}{N_i} \quad \text{(Equation 2)}$$

$$N_i = A(\Delta\sigma)^{-3} \quad \text{(Equation 3)}$$

In [29], gate component stress ranges from the finite element simulations were analyzed using the AASHTO nominal stress approach and fatigue damage within each high stress region was evaluated to determine the critical region susceptible to fatigue. Following determination of the critical region, various levels of prestress were applied to the critical section (Section F13 in Figure 2) to determine the effect of a prestressed retrofit on the resulting component stress ranges. As shown in Figure 4, the fatigue stress range in the finite element model shifted as the prestress force increased. This is unsurprising; however, it is interesting that with moderate levels of prestress, component stress ranges were shifted such that a portion of the stress range moved into compression, reducing both the applied mean stress and the stress range amplitude (as only a portion of the compressive cycle is considered damaging).

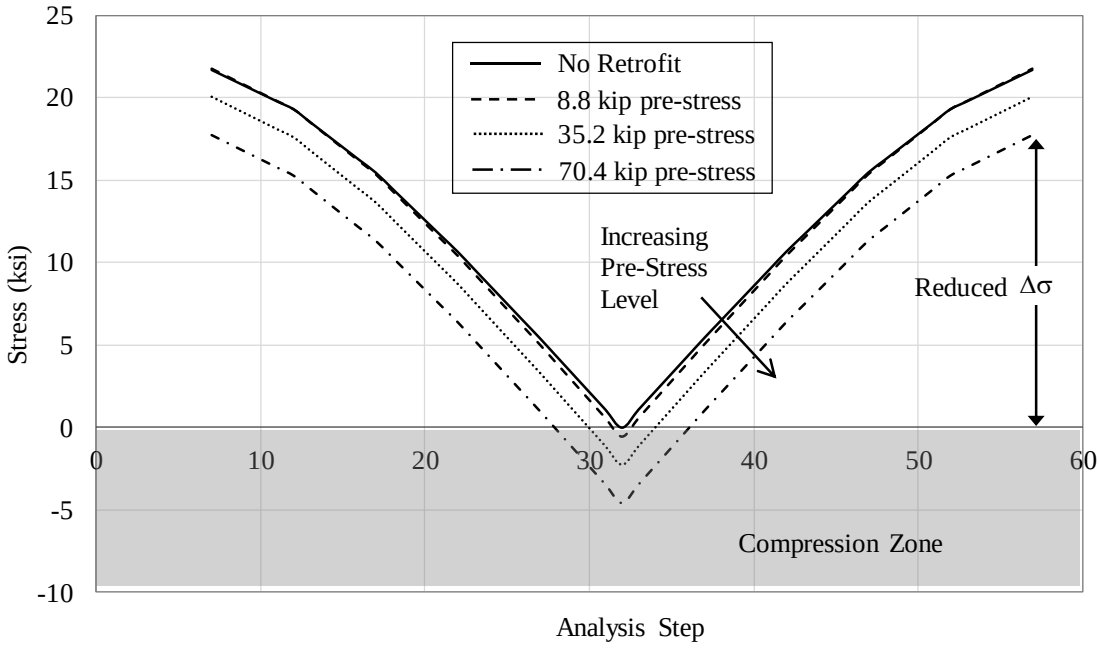

Figure 4. Gate component stress shift due to various prestress levels [29]

Rather than arbitrarily prestressing the gate components for an arbitrary fatigue life improvement, [29] then used the Goodman local stress approach to determine the level of prestress required to shift the gate component stress state into a region of infinite life. Figure 5 from [29] shows the resulting gate component stress state and the considered Goodman diagram. Note that the stress-state in Figure 5 is nowhere near the fatigue threshold value required for infinite life, even after an applied prestress of 35.2kips. From Figure 5, [29] determined that an impractically large prestress of 366.6kips is required to shift the stress-state into the infinite life region.

This thesis builds upon the work of [29] by developing a CFRP prestressing strategy for lock gate components, and experimentally investigates the effectiveness of prestressing strategies on controlling fatigue demands. The following sections describe the development of a retrofit prototype, including CFRP prestressing strategies, bonding mechanisms, and longer-term prestress performance (creep/relaxation). Additionally, a series of large-scale fatigue experiments are discussed and the effectiveness of the retrofit on controlling local fatigue demands is presented.

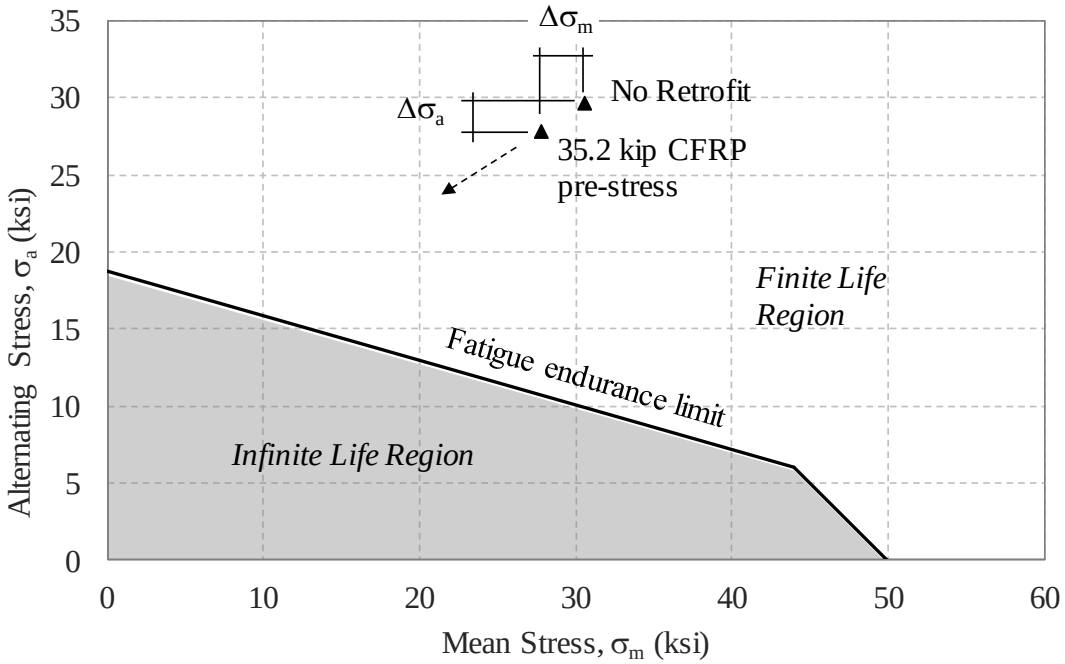

Figure 5. Effect of prestress on critical region stress state using modified Goodman diagram [29]

3. Development of a Fatigue Retrofit Prototype

While the prestress required for infinite fatigue life in [29] may be impractically large for a retrofit scenario, the analyses in [29] indicate that moderate prestress levels are capable of significantly extending gate fatigue life (8.6 year extension at 32.5kip prestress). In the retrofit development of this study, the prestress is chosen to be applied through CFRP plates; however, corrosion precautions must be taken because the CFRP material functions as the cathode in the galvanic reaction with the low-carbon steel anode, promoting steel corrosion. To avoid negative corrosion effects from the retrofit on the lock gate component, the CFRP in the retrofit will need to avoid contact with any gate components (forcing an un-bonded CFRP retrofit application).

To develop prestress within the CFRP material and transfer the prestress into the gate component, a friction clamping mechanism is designed. Figure 6 shows the prototype clamping mechanism considered for the prestressed retrofit along with the retrofit assembly steps. In Figure 6, the CFRP material is clamped between two steel plates (T-plates in Figure 6) which fit within another box clamp that is attached to the gate specimen. In Figure 6, the T-plate clamps that hold the CFRP are free to move longitudinally within the box clamp. The retrofit prototype developed in this project is made of A36 steel; however, in the lock environment a galvanic protection layer (such as corrosion resistant paint or metallic coating) between the steel retrofit and CFRP will need to be added to prevent galvanic action within the retrofit itself. The CFRP prestress is applied by tightening bolts as seen in Figure 7, which allows the T-plates holding the CFRP (part b) to move relative the box clamp (part a) which is attached to the gate specimen (thus inducing a prestress).

At a minimum, the retrofit uses a friction-grip clamping mechanism to keep the CFRP plate from slipping; however, in order to achieve high levels of prestress, additional bonding

mechanisms may be needed. The next section investigates several CFRP-to-steel bonding strategies to achieve high levels of prestress.

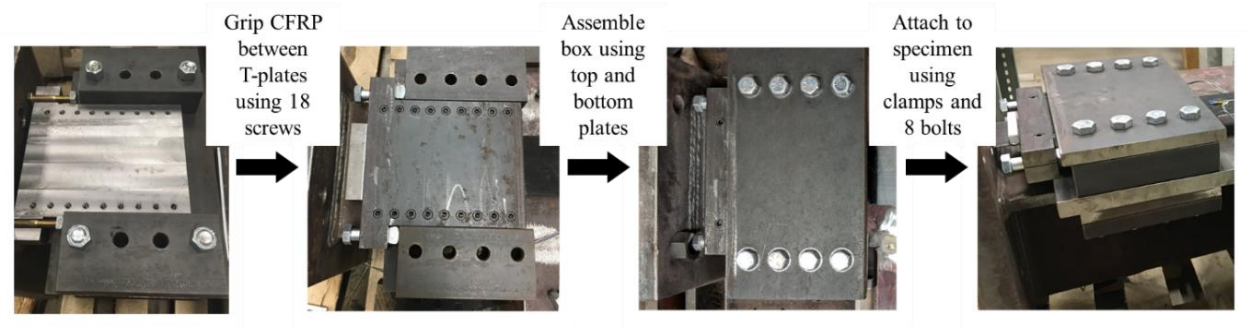

Figure 6. Retrofit components and assembly steps for the CFRP retrofit

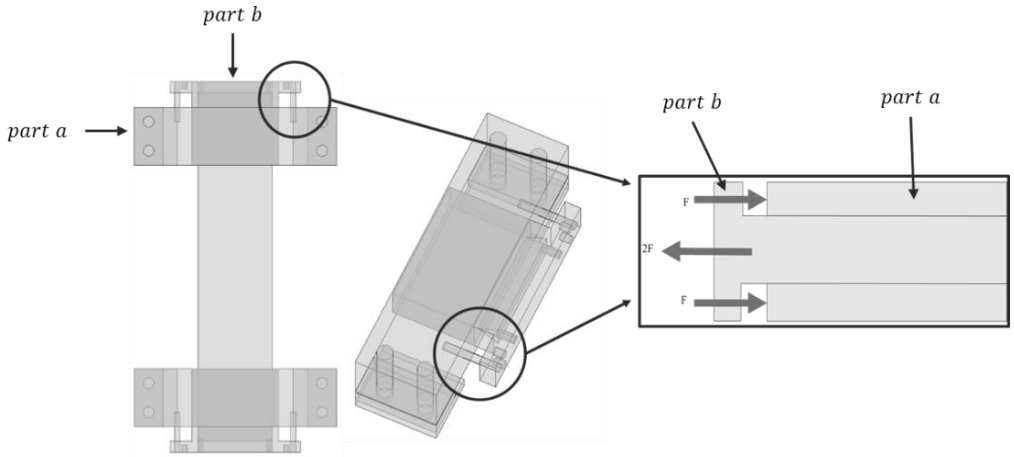

Figure 7. Cross-section of prestress bearing mechanism with forces applied by bolts to create the prestress [29]

3.1. *Investigation into Retrofit Bonding Strategies for Achieving Desired Prestress Levels and Preventing Prestress Losses*

In order for the retrofit to be effective in reducing stresses within the critical gate components, the induced CFRP prestress must be maintained over long durations of time. To investigate the available prestress that can be applied and to understand any prestress losses due to relaxation and creep of the retrofit materials, bonding experiments were conducted for both static slip and longer duration prestress losses. In this study four bonding mechanisms in addition to the bare-steel friction clamps were considered: 1) wedge grips to provide additional clamping of the

CFRP, 2) sandpaper to increase the surface roughness and coefficient of friction between the CFRP and steel clamping plates, 3) epoxy adhesion between the steel and CFRP surfaces, and 4) a proprietary Slipnot^{TM} roughened surface created by spraying molten steel on the retrofit clamping surfaces. Figure 8 shows the retrofit clamps with each of the four additional bonding strategies considered.

For each bonding experiment, the CFRP plates and gate component steel surface were instrumented with uni-directional strain gauges for measuring local strains. This allowed prestress levels within the CFRP to be calculated and comparisons between the bonding mechanisms to be made. For each bonding mechanism considered, the initial maximum prestress was obtained by applying increasing prestress levels to the CFRP until the bonding failed (as indicated by a sudden drop in CFRP strain from the gauge readings [see Figure 9]).

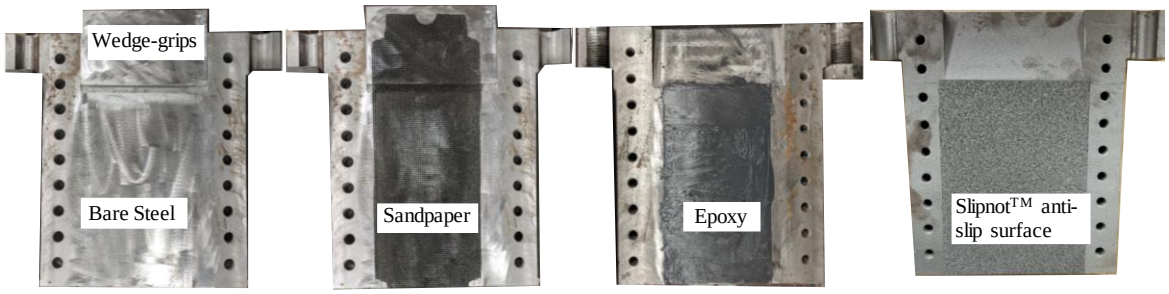

(a) (b) (c) (d)

Figure 8. Four bonding mechanisms for clamping the CFRP consisting of: (a) wedge grips, (b) sandpaper, (c) epoxy, and (d) Slipnot^{TM} surface.

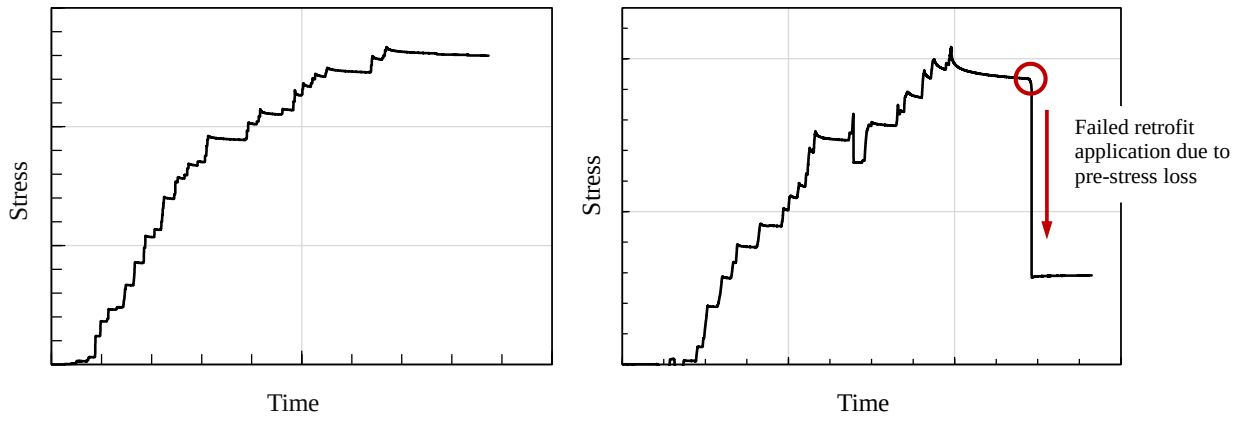

(a) (b)

Figure 9. Representation of CFRP stress data showing prestress loss due to bond failure.

Table 1 shows the experimental matrix for the bonding experiments, along with the maximum CFRP prestress level achieved. From Table 1, the experiment with only the bare-steel bolted plates achieved 5.03ksi of CFRP prestress prior to initiation of slip between the CFRP and steel surface. By adding the wedge grips, which are designed to clamp the CFRP prior to slip, the maximum prestress achieved at slip was 34.3ksi (nearly seven times that of the bare steel clamps). Additional testing with the clamping wedges and added sandpaper achieved only 15.3ksi of prestress as the flexibility of the sandpaper layer actually reduced the friction between the steel and CFRP. The highest CFRP prestress levels were achieved by using adhesive epoxy to bond the CFRP to the steel clamps. By using an epoxy bond, a CFRP prestress of 52.8ksi was achieved without the CFRP slipping (over ten times that for the bare steel clamped plates). This indicates that the epoxied CFRP bond would likely be able to achieve even higher prestress levels.

Figure 10 shows the prestressing results for the various bonding strategies considered. In Figure 10, it can be seen that the wedge-grip bonding strategy slipped at a CFRP prestress of 34.3ksi while the combined sandpaper and wedge-grip strategy performed worse (only reaching 15.3ksi). From Figure 10, the Slipnot^{TM} and epoxied surfaces performed the best, each being able

to achieve more than 50ksi of CFRP prestress. Even though there are similarities in performance between the Slipnot™ and adhesive, a decision was made to proceed with epoxy for the remainder of the structural testing.

Table 1. Test variations to confirm bond mechanism

Bonding Test No.	Plate Clamps	Wedges	Sandpaper	Epoxy	Slipnot™ Surface	Prestress (ksi)
BT-1	X					5.03
BT-2	X	X				34.3
BT-3	X	X	X			15.3
BT-4	X	X		X		52.8
BT-5	X				X	53.8

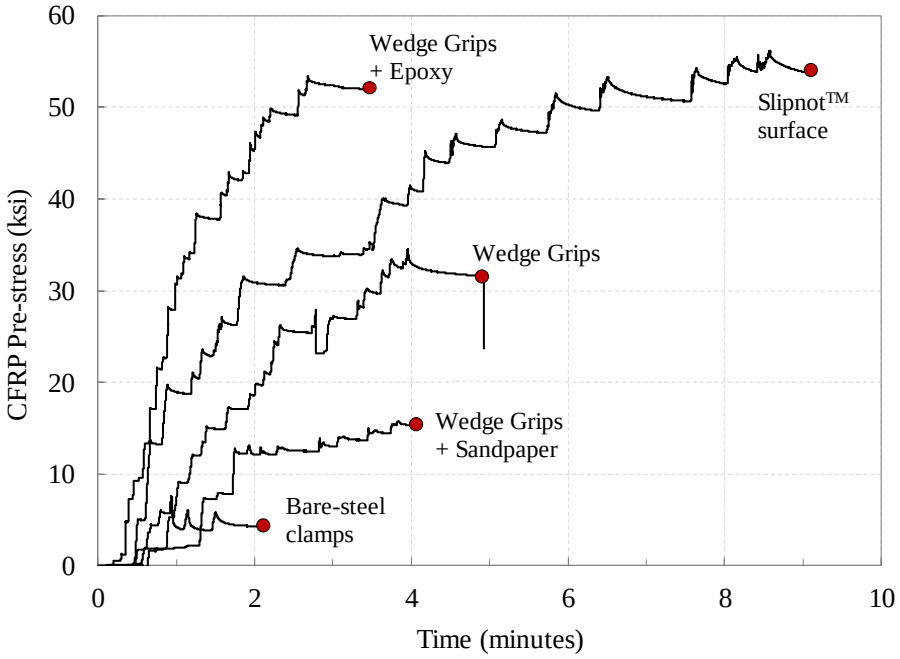

Figure 10. CFRP prestress measurements from the different bonding mechanisms considered

While the initial prestress capabilities of the epoxy bonding was chosen based on the initial prestress tests, the long-term effects of prestress loss, specifically creep and relaxation, must be understood to gauge long-term retrofit performance. Long-term tests extended from the static slip tests if there was no failure of the bonding strategy, see Figure 9, which consisted of sandpaper and epoxy. Figure 11 shows the initial prestressing of the epoxied CFRP retrofit, along with the

long-term monitoring of prestress losses. From Figure 11, a slight initial prestress loss is observed within the first few minutes. This prestress loss gradually decayed resulting in a total prestress loss of 5.52ksi (approximately 10%) after 14 days. For comparison, prestress losses within the un-epoxied wedge retrofit using sandpaper saw a prestress loss of 1.95ksi (approximately 12%) after 3 days possibly due to the compressibility of the sandpaper.

Because the ambient room temperature can have an effect on prestress measurements, room temperature was recorded during the long-term testing. Figure 12 shows the relationship between CFRP prestress and ambient room temperature during testing of the epoxy-bonded retrofit. In Figure 12, small peaks in CFRP prestress correspond to slight decreases in room temperature.

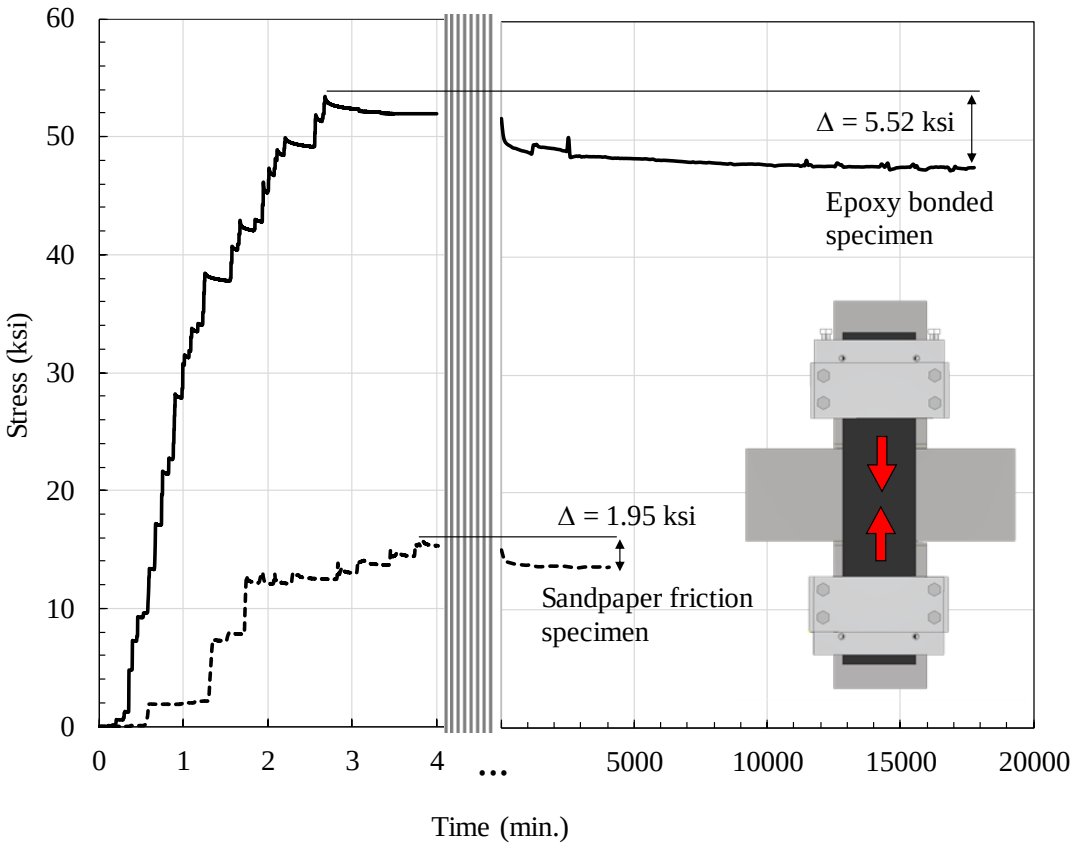

Figure 11. Measured CFRP prestress losses due to relaxation and creep.

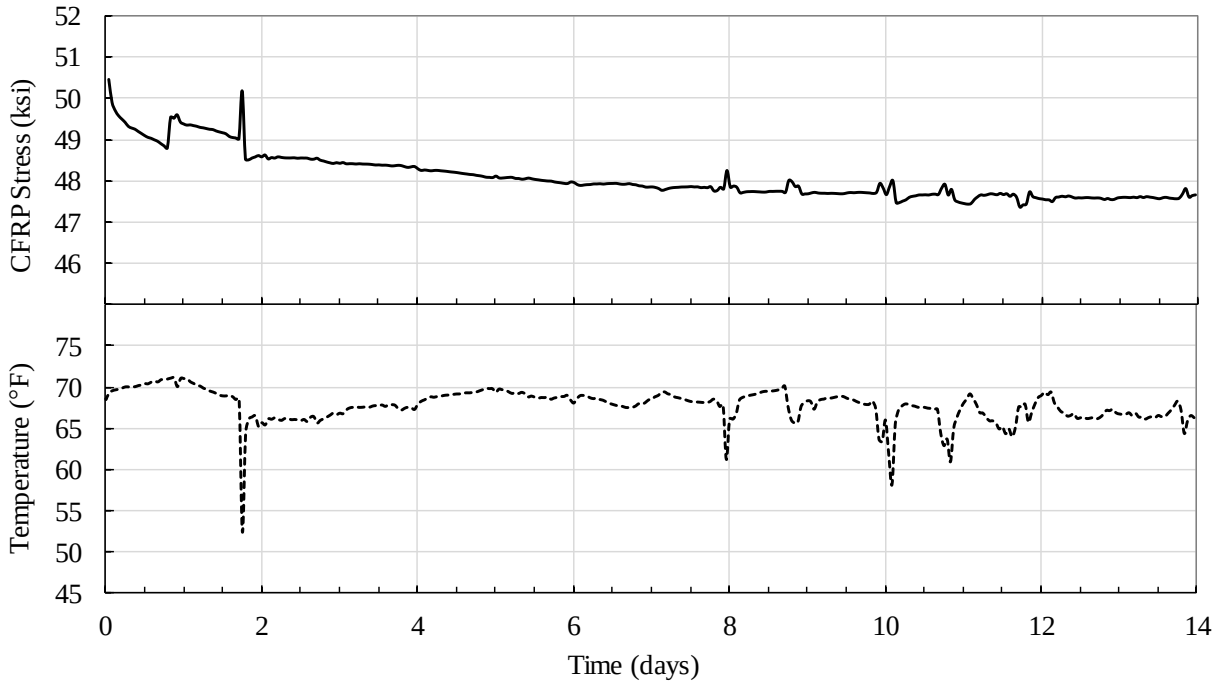

Figure 12. Measured temperature effects on CFRP prestress levels.

4. Experimental Investigation into Retrofit Fatigue Mitigation

To verify the effectiveness of the prestressing strategy and evaluate the performance of the developed retrofit, seven experimental fatigue tests were conducted. The following sections describe the seven experimental tests, including the test specimen geometry, loading, experimental setup, and instrumentation, followed by a discussion of the testing results.

4.1. *Specimen Geometry*

Two specimen geometries were considered in the experimental program, one representing a full-scale component geometry and one representing a half-scale component geometry of only the gate faceplate. The full-scale specimen geometry is identical to Section F13 described in Section 2 and is fabricated from design details of the Greenup Lock and Dam provided by the United States Army Corps of Engineers. Shown in Figure 13(a), the full-scale test specimen is 36 inches by 30in. by 10-3/4in., representing a section of gate near the critical region. Two different

weld types join the full-scale test specimen plates. As shown in Figure 13(a), the welds consist of double-sided 3/4in. bevel welds and 5/16in. fillet welds. The specimen is designed with two attachment plates connected to each end as seen in Figure 13. These attachment plates are 2in. in thickness to avoid prying effects that cause unwanted stresses on the connections to the frame instead of strictly tensile forces on the specimen. Figure 13(b) shows the half-scale specimen dimensions and fabrication details.

All gate specimens tested were notched near the plate intersection welds (see Figure 14) using abrasive cutting discs prior to testing. These notches were added to the specimens to induce local stress concentrations (simulating gate component damage) and to create a worsened fatigue condition.

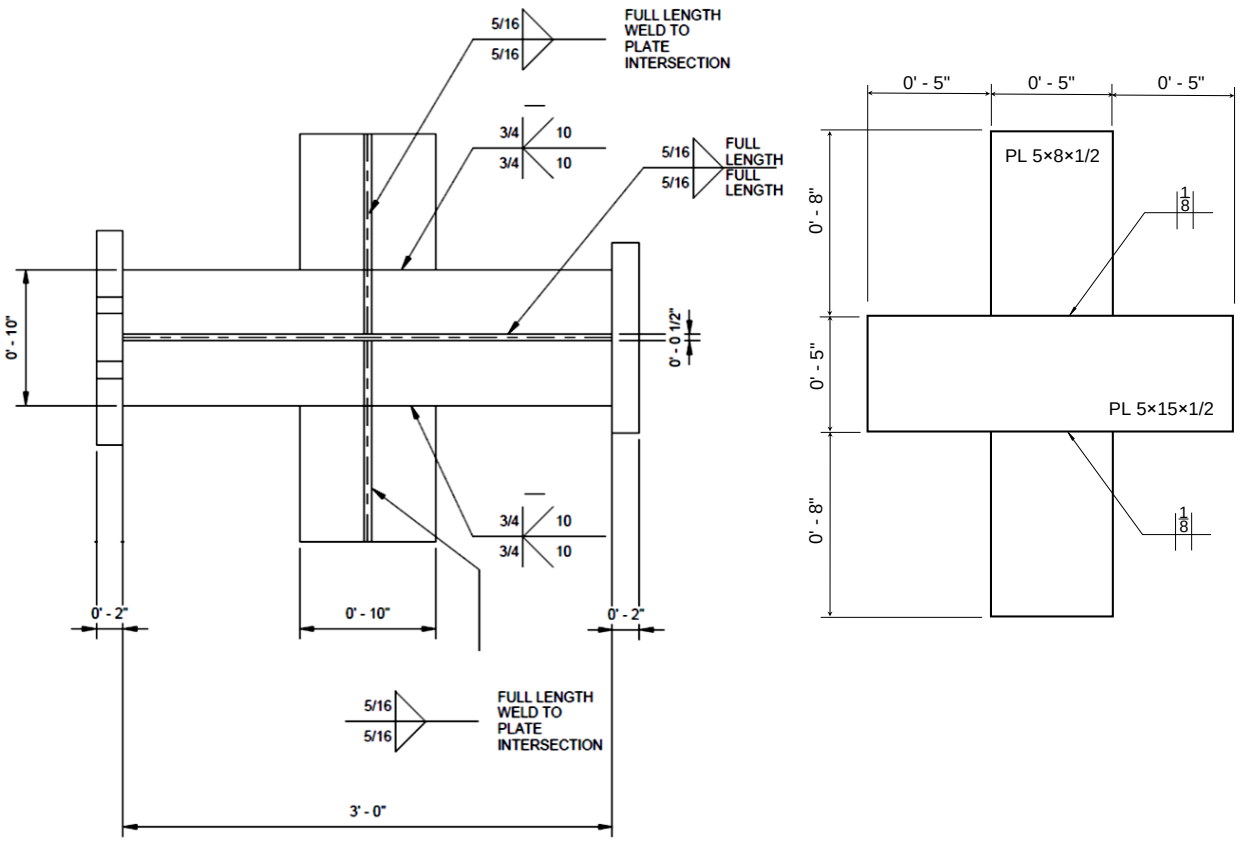

(a) (b)

Figure 13. Gate section F13 fabrication details for (a) full-scale specimen and (b) half-scale specimen

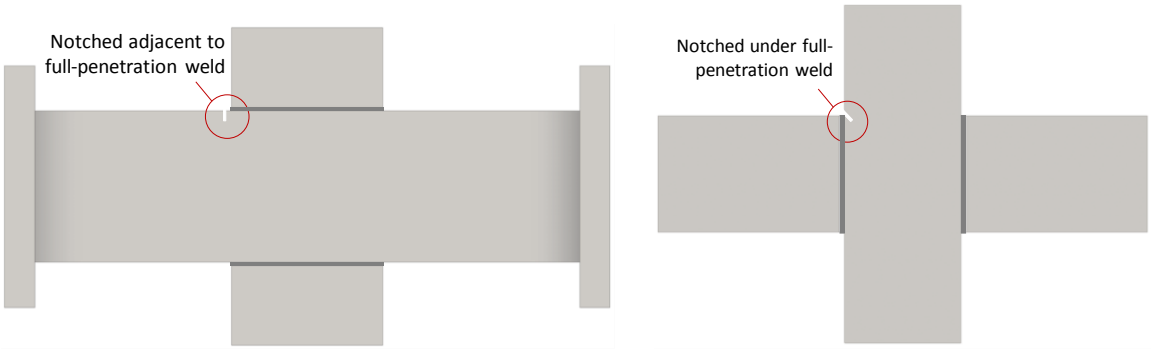

(a) (b)

Figure 14. Notch location for (a) full-scale specimen and (b) half-scale specimen.

It is important to note that for the resulting fatigue calculations, this notching reduces the Goodman criteria by dividing the endurance strength, S_e, by a fatigue notch factor, K_f, which is based on the geometry and the elastic stress concentration factor, K_t, of the specimen. The elastic stress concentration factor, K_t, can be calculated from the derived equation shown below [31] which considers the ratio between the depth of the notch, d, and the radius of the notch, r, as shown in Table 2.

$$K_f = 1 + \frac{K_t - 1}{1 + \sqrt{\frac{\rho}{r}}} \qquad \rho = \frac{104MPa}{S_{ult}}$$

$$K_t = C_1 + C_2\left(\frac{d}{w}\right) + C_3\left(\frac{d}{w}\right)^2 + C_4\left(\frac{d}{w}\right)^3$$

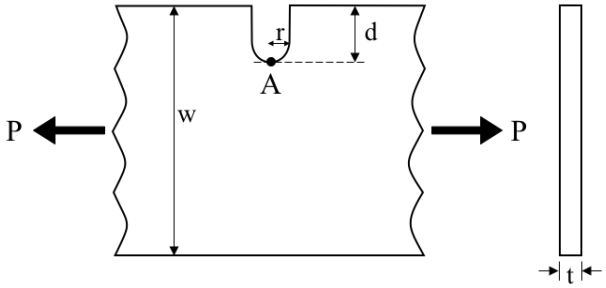

Table 2. Coefficients for stress concentration factor [31]

	$0.5 \leq d/r < 2.0$	$2.0 \leq d/r \leq 20.0$
C1	$0.907 + 2.125\sqrt{d/r} + 0.023\,h/r$	$0.953 + 2.136\sqrt{d/r} - 0.005\,h/r$
C2	$0.710 - 11.289\sqrt{d/r} + 1.708\,h/r$	$-3.255 - 6.281\sqrt{d/r} + 0.068\,h/r$
C3	$-0.672 + 18.754\sqrt{d/r} - 4.046\,h/r$	$8.203 + 6.893\sqrt{d/r} + 0.064\,h/r$
C4	$0.175 - 9.759\sqrt{d/r} + 2.365\,h/r$	$-4.851 - 2.793\sqrt{d/r} - 0.128\,h/r$

Figure 15 shows how adding notches to the gate specimens reduces the component fatigue endurance limit (see the downward shift of the Goodman line after notching). In Figure 15, it is possible for a notched component to have a finite fatigue life under the same loading conditions that would produce an infinite fatigue life for an un-notched (smooth) component.

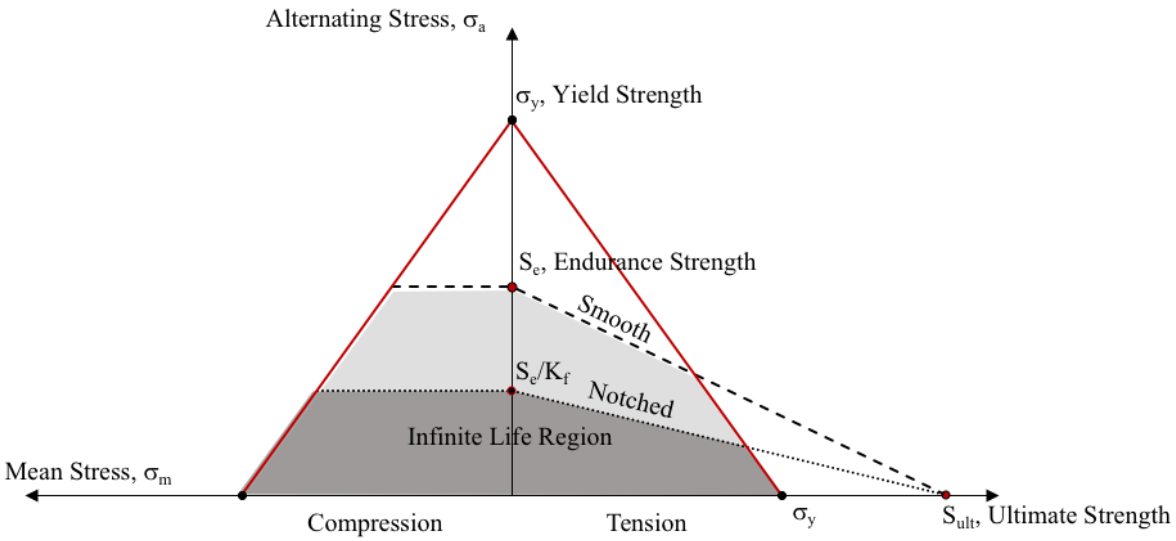

Figure 15. Constant life diagram using the modified Goodman criteria for smooth and notched specimens

4.2. *Loading*

Constant amplitude unidirectional tensile loading (where the specimen is loaded and unloaded during each cycle) is considered in this study. The loading is intended to simulate similar stress distribution patterns within the gate component during hydrostatic pressure changes that occur during lock operation. To maintain a constant amplitude nominal stress within the component, all specimens are loaded in force-control. Figure 16 shows the three loading configurations with configuration 1 (C1) representing axial loading of the full-scale gate specimens parallel to the joint welds, configuration 2 (C2) representing bending and shear loading within the full-scale gate specimens, and configuration 3 (C3) representing axial loading of the half-scale specimens perpendicular to the joint weld. It should be noted that during normal gate operation, the gate component feels a combination of bending, shear, and axial load; however, due to limitations with large-scale testing, each of the loading conditions are considered separately.

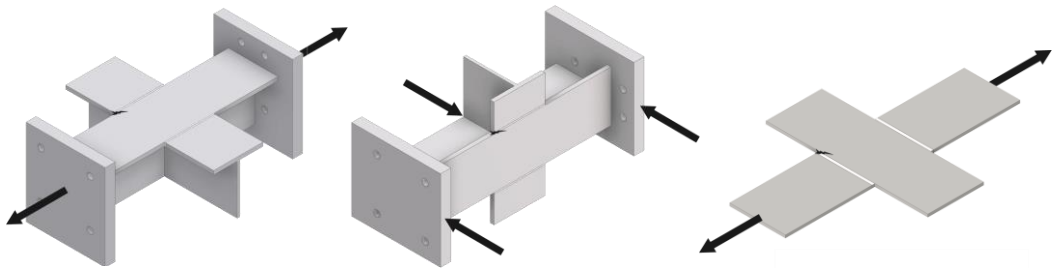

(C1) (C2) (C3)

Figure 16. Specimen loading configurations for the full scale component tests (C1 and C2) and the half-scale component tests (C3)

To verify that the loading of the test specimens creates a similar stress state observed during gate operation, a simulation of each test specimen loading was performed. Boundary conditions similar to those imposed by test configurations C1 and C2 are shown in Figure 17, along with a comparison of stress contours between the full gate model and experimental setups. From Figure 17, similar stress concentrations are observed at the test specimen corners while larger stresses are observed near the center of the plate. These larger stresses near the plate center are of less concern from a fatigue standpoint. The stresses near the plate center in the gate model likely differ somewhat from the two test configurations due to the bi-directional bending condition experienced during gate operation. Contours presented in Figure 17 confirm that the two loading configurations impose similar stress conditions near the plate intersection corners.

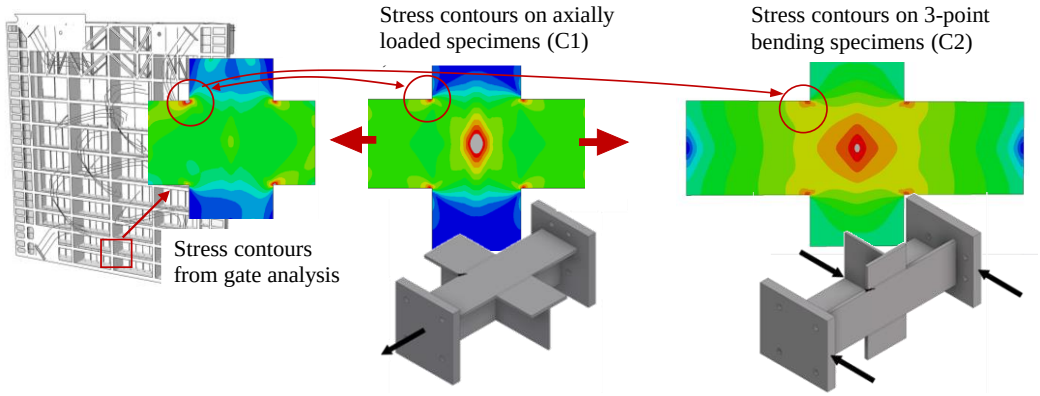

(a) (b)

Figure 17. a) Stresses from submodel of lock gate; b) Stresses from model of test specimens

4.3. *Experimental Setup and Testing Matrix*

A total of three full-scale component fatigue tests were conducted on notched gate components to measure the effects of the retrofit strategy near regions of high stress concentration. The full-scale tests consider two loading configurations which induce both axial and flexural stresses in the gate component. Figure 18(a) and Figure 18(b) show the experimental setup for the full-scale testing, consisting of a self-reacting frame, servo-hydraulic actuator, and full-scale gate component specimen. A photograph of the full-scale test setup is also shown in Figure 19(a). The self-reacting frame used to load each gate specimen (shown in Figure 18 and Figure 19) was stiffened for this study to reduce deflections during loading therein allowing higher frequency loadings. The reaction frame consists of two W12×210 beam sections connected to four W12×120 column sections. For axial loading, the specimen is connected to both the actuator and reaction frame (providing an axial load path that must travel through the specimen) with four high-strength 1-1/4" A490 bolts (see Figure 18(a)). For flexural loading, the specimen is subjected to three-point bending subjecting the face of the gate specimen near the critical region to both tension and flexure (see Figure 18(b)).

In addition to the full-scale tests, four half-scale fatigue tests were conducted to investigate alternative specimen orientations and the effectiveness of the prestressed retrofit on fatigue crack mitigation. Unlike the full-scale specimens, all half-scale specimens are tested in a Walter+Bai servo-hydraulic bi-axial fatigue testing machine capable of providing rapid fatigue cycles. Figure 18(c) shows the half-scale testing configuration and Figure 19(b) shows a photograph of the half-scale specimen during testing. Table 3 presents the experimental testing matrix, outlining the specimen names, retrofit condition, loading type, applied force range, and retrofit prestress level (if applicable).

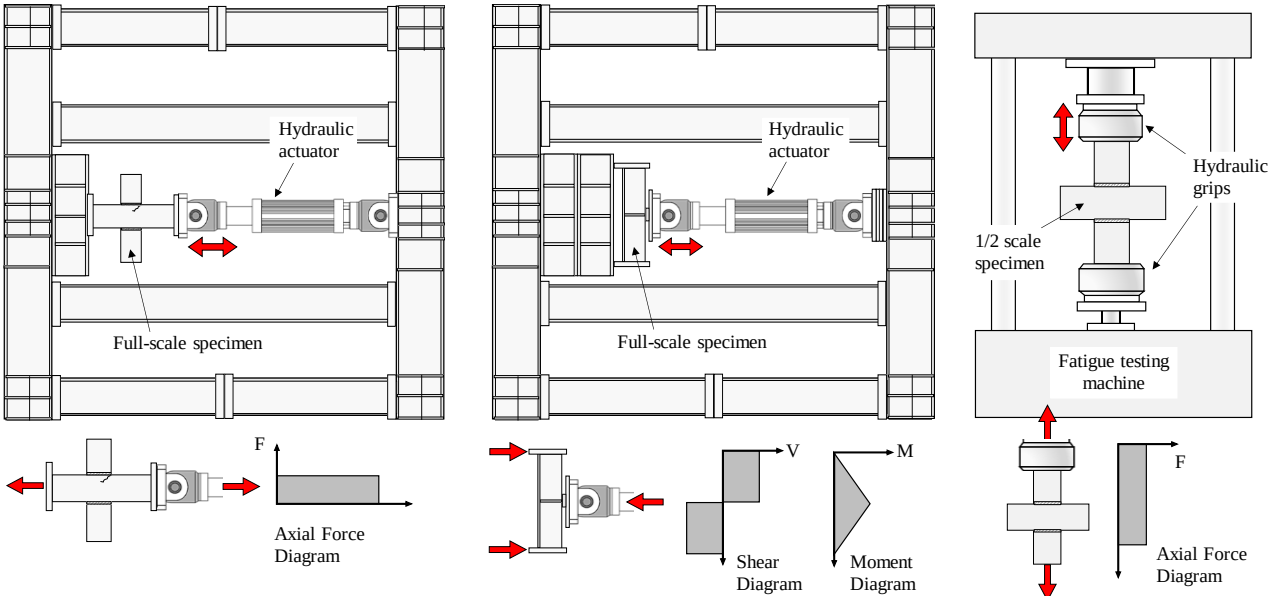

Figure 18. Experimental test setup and specimen force diagrams for (a) full-scale axially loaded specimen, (b) full-scale specimen in three-point bending, and (c) half-scale axially loaded specimen.

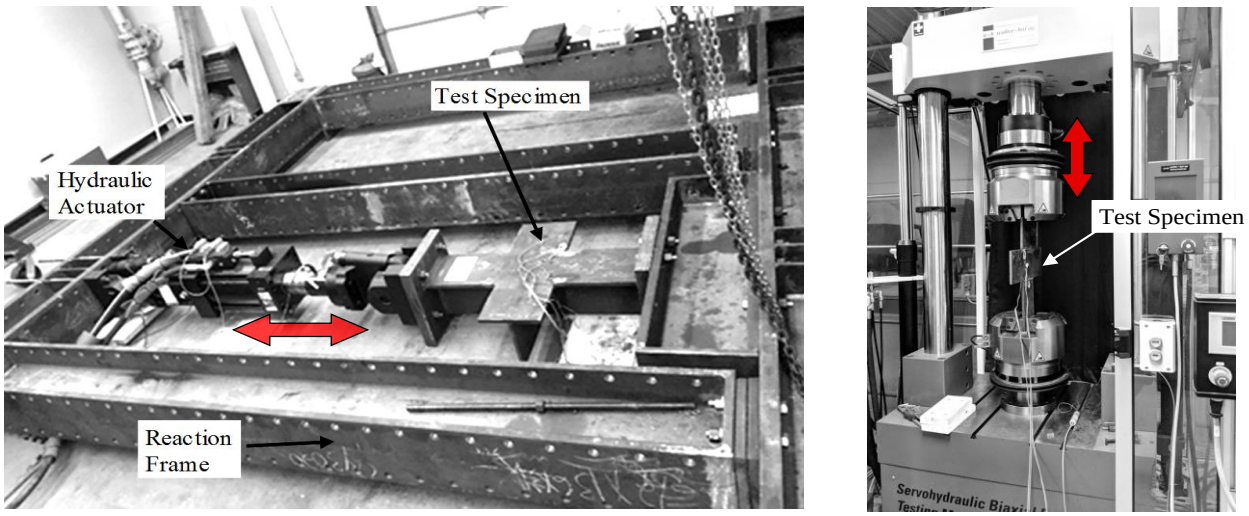

Figure 19. Photograph of experimental setup for (a) full-scale testing in the large reaction frame and (b) half-scale testing in the Walter+Bai servo-hydraulic bi-axial fatigue testing machine.

Table 3. Experimental test matrix

Experimental test No.	Retrofit (Y/N)	Loading type	Loading frequency (Hz)	Applied force range (kips)	Applied retrofit prestress level (ksi)
C1-1	N	Axial	2 – 6	50 – 80	--
C2-1	N	3-point	2 – 6	80	--
C2-2	Y	3-point	2 – 6	80	7.3 – 17.3
C3-1	N	Axial	2	19.6	--
C3-2	Y	Axial	2	19.6	7.2 – 18.0
C3-3	N	Axial	2 – 8	19.6	--
C3-4	Y	Axial	2 – 8	19.6	13.65

4.4. *Instrumentation and Monitoring*

Each experimental specimen was instrumented with multiple strain gauges to monitor local component stresses during loading. These gauges were located near the notched regions to measure local stress concentrations resulting from the geometry discontinuities, as well as regions away from any local influences to measure nominal specimen stresses. Figure 20 shows the orientation and location of instrumentation for the C1, C2, and C3 specimen configurations. Note that gauges are provided on both sides of the steel plate to allow for separation of measured bending and axial stresses.

In addition to the instrumentation, non-destructive monitoring techniques were used to identify and track the presence of fatigue cracking. The crack detection method used in this study involves visual inspection aided by dye penetrant. It should be noted that while the dye penetrant was the primary means for identifying crack initiation, post-test analysis of the strain gage data also helped in identifying the presence of cracking through measurement of local force changes.

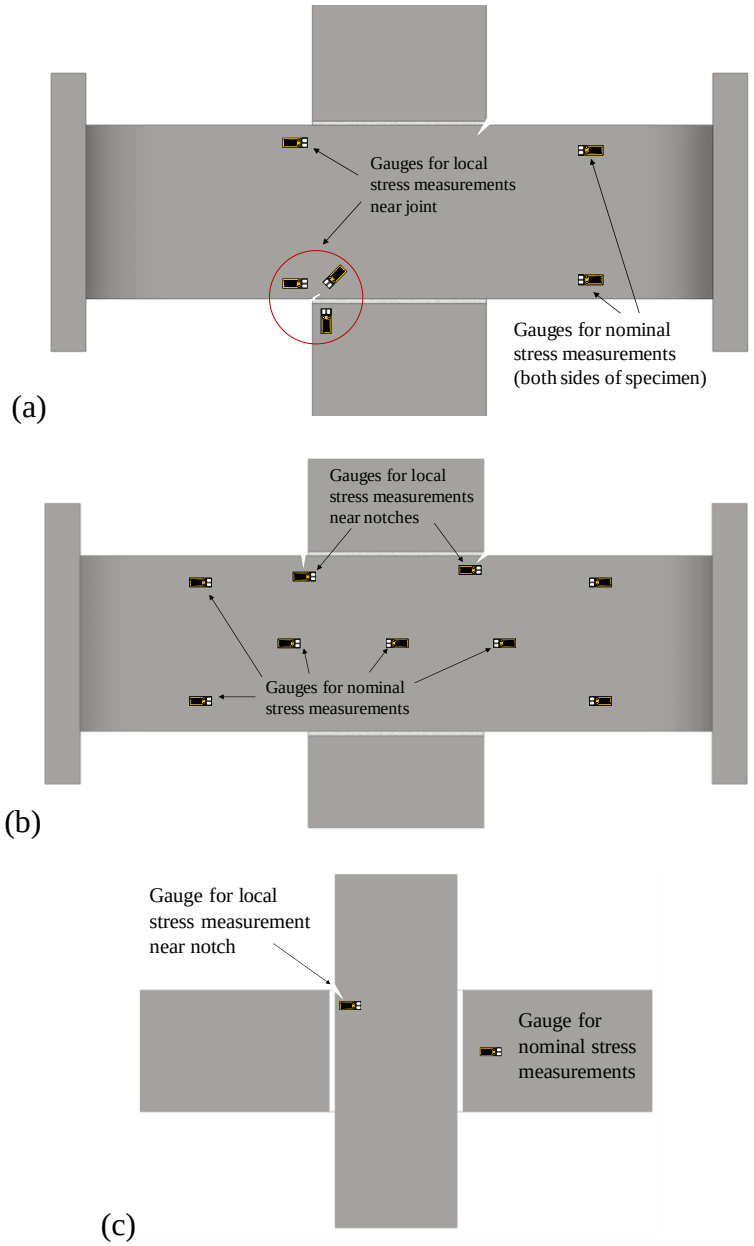

Figure 20. Strain gauge instrumentation locations for: a) full-scale configuration 1 (C1), b) full-scale configuration 2 (C2), and c) half-scale configuration 3 (C3).

4.5. *Experimental Fatigue Test Results*

4.5.1. Testing Observations from Full-Scale and Half-Scale Specimens

As mentioned in the description of specimen geometry, all specimens were notched near a weld corner to aid in crack initiation and simulate poor detailing (common in many existing gate components). Preliminary testing was conducted on specimen C1-1 to measure the effect of this

notching on the local stress-state near the connection weld region. Figure 21 compares the pre- and post-notch stresses within the connection region of specimen C1-1 which indicates that the notching increases the local stress state by more than 4.5 times. Note that the gauge results presented in Figure 21 are averages between gauges on the top and bottom plate sides (to isolate axial strains). By comparing the top and bottom longitudinal gauges in Figure 21(a), It can be observed that the experimental loading induced slight lateral bending in the specimen (note that the solid line from the top gauge is larger than the dashed line from bottom gauge).

Following notching of specimen C1-1, a total of 13,730,163 fatigue cycles were applied at a force range of 50kips with no observable fatigue cracking near the notch. Strain measurements near the notch remained stable throughout the test and resembled those shown in Figure 21(b) indicating no fatigue cracking. Additional dye-penetrant testing near the notch helped confirm no fatigue cracking by visual inspection. Due to the significant time required to generate a fatigue crack, it was decided to conclude the axial loading fatigue test and focus on the three-point bending specimen configuration capable of producing higher stresses within the gate specimens.

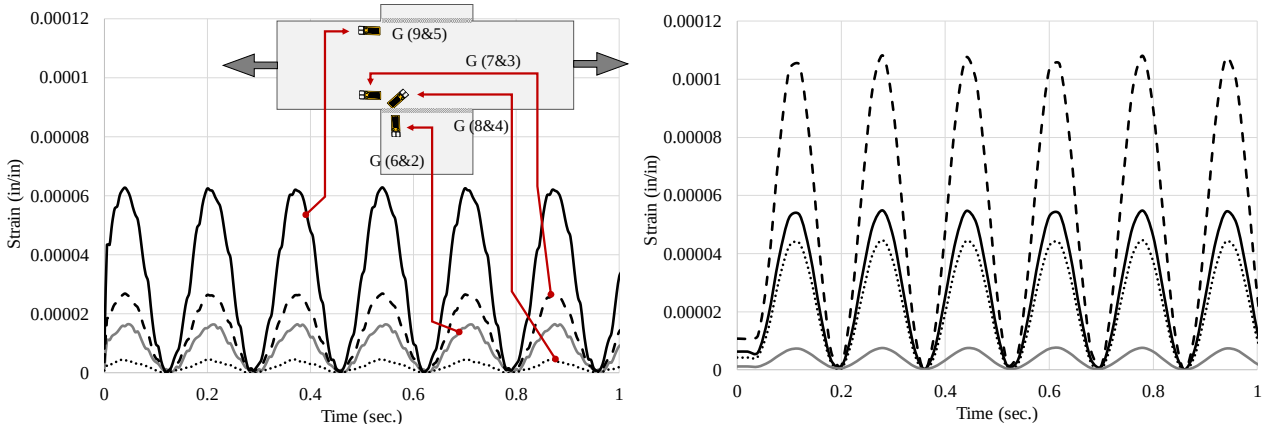

Figure 21. Recorded strains, a) pre-notch; b) post-notch

The goal of the initial fatigue testing with specimens C1-1 and C2-1 was to induce a sharp fatigue pre-crack to investigate retrofit effectiveness; however, similar to specimen C1-1,

specimen C2-1 (loaded in three-point bending at a force range of 80kips) was subjected to 4,598,234 fatigue cycles with no observable fatigue crack forming at the notch. Rather than continue with the fatigue crack initiation experiments, it was decided to use the local stress concentration from the induced notch to investigate the local stress effects of the prestressed retrofit. Table 4 shows the additional cyclic tests conducted (C2-2, C3-1, and C3-2) to provide comparison between local notch stress states without and with various levels of CFRP prestress. Tests C3-3 and C3-4 were added half-scale fatigue tests to measure resulting fatigue-life improvements and will be discussed in a later section.

Table 4. Experimental test matrix and resulting fatigue cycles applied

Experimental test No.	Retrofit (Y/N)	Loading type	Retrofit prestress level (ksi)	Number of applied fatigue cycles
C1-1	N	Axial	--	13,730,163
C2-1	N	3-point	--	4,598,234
C2-2	Y	3-point	7.3-17.3	N/A
C3-1	N	Axial	--	N/A
C3-2	Y	Axial	7.2-18.0	N/A
C3-3	N	Axial	--	989,235
C3-4	Y	Axial	13.65	2,911,198

4.5.2. Effect of Retrofit Prestress Levels on Specimen Local Stresses

The applied CFRP prestress is capable of reducing the local stress felt at the notch of both the full-scale and half-scale specimens. Table 5 presents the three full-scale and four half-scale experiments having varied levels of CFRP prestress. In Table 5, prestress levels ranging between 7.3 and 17.3ksi were able to reduce the full-scale component mean stress by between 4 and 8.3ksi. Additionally, the prestress was able to reduce the stress-amplitude of the full-scale notch stress by between 1.6 and 2.3ksi. Similar results were observed for the half-scale experiments, with prestress levels between 7.2 and 18ksi reducing the component mean stress by between 2.5 and 5.4ksi respectively. The reduction in mean stress and stress-amplitude at the notch directly

translates to increased fatigue life. Figure 22 shows the effect of prestress level on stress-range and mean stress for the full-scale experiments. In Figure 22, a noticeable downward shift can be seen as the prestress level in the CFRP is increased.

Table 5. Mean and amplitude stress shift due to CFRP prestress level

Specimen Type	Applied force range (kips)	Retrofit prestress level (ksi)	Reduction in component mean stress (ksi)	Reduction in component stress amplitude (ksi)
Full-Scale	80	7.30	4.0	1.6
Full-Scale	80	14.8	7.7	2.2
Full-Scale	80	17.3	8.3	2.3
Half-Scale	19.6	7.20	2.5	0.7
Half-Scale	19.6	10.6	3.4	1.2
Half-Scale	19.6	12.5	4.0	1.5
Half-Scale	19.6	18.0	5.4	2.3

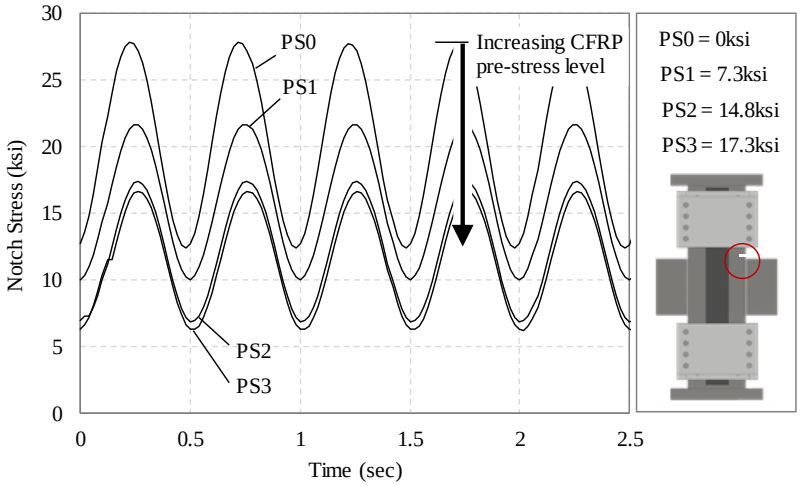

Figure 22. Effect of CFRP prestress on local notch stress state.

As the specimen notch stress is reduced, the stress-state moves closer to the infinite life region. For the full-scale and half-scale experiment, the resulting shift in notch stress state relative to the notched Goodman criterion is shown in Figure 23 and Figure 24 respectively. As shown in Figure 23, the 8.3ksi reduction in mean stress at a prestress of 17.3ksi shifts the notch stress-state near the border of the fatigue threshold line, but remains within the finite life region. This indicates

that a fatigue life improvement is likely made; however, the component will eventually be subject to fatigue cracking. Similar results were noticed for the half-scale specimens which remained within the finite life region after achieving a mean-stress shift of 5.4ksi at 18ksi prestress. The following section quantifies the effect of this mean stress shift on the resulting half-scale component fatigue life.

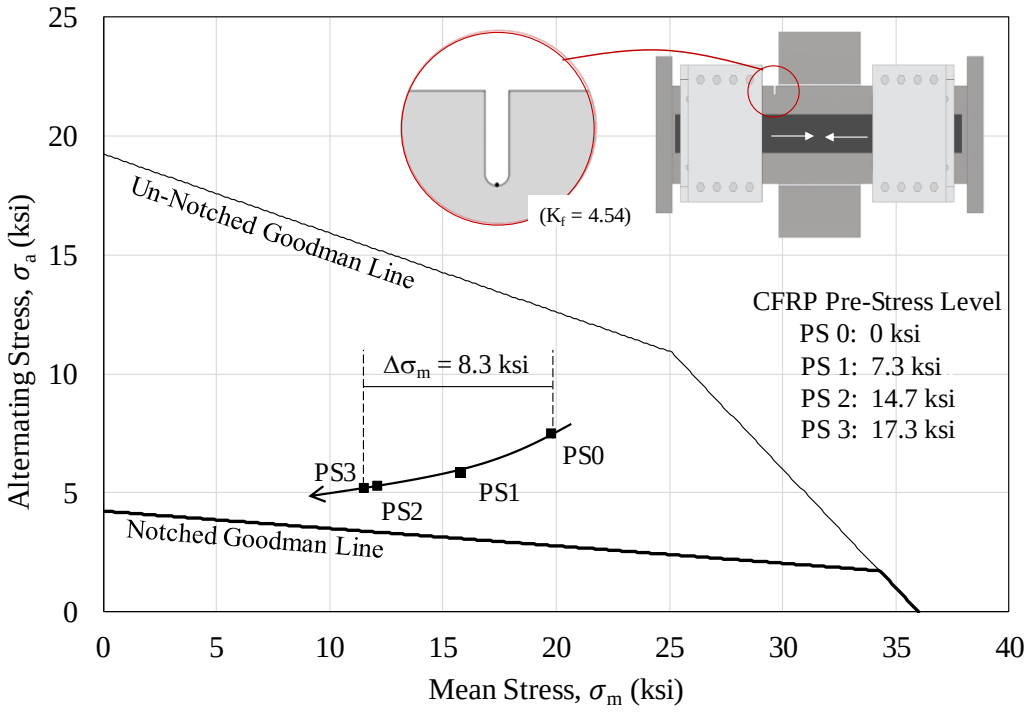

Figure 23. Effect of CFRP prestress level on full-scale component stress state

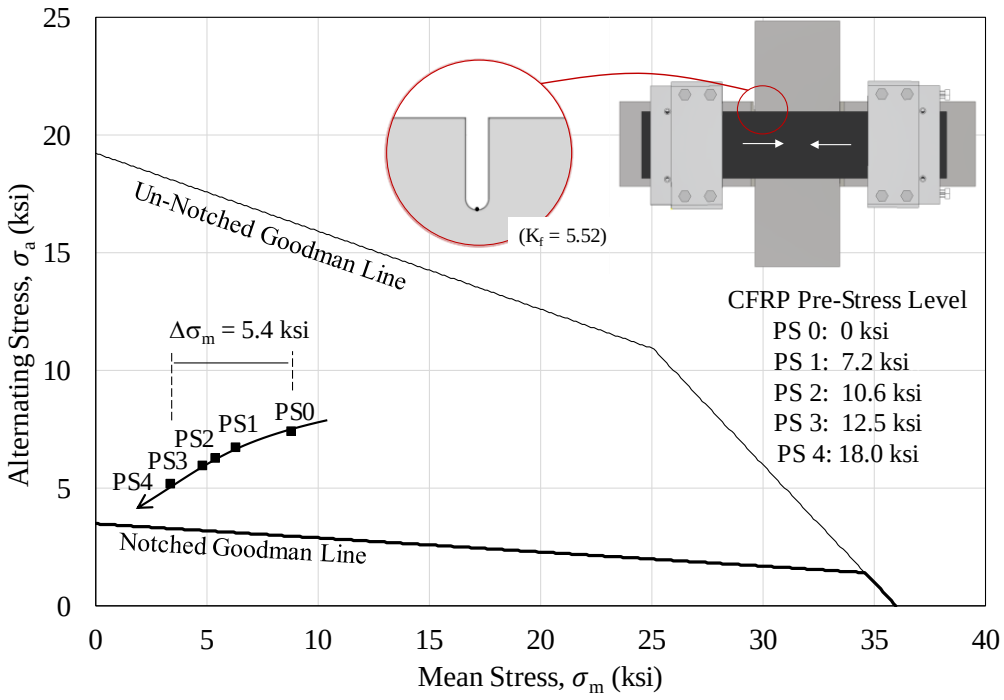

Figure 24. Effect of CFRP prestress level on small-scale component stress state

4.5.3. Effect of Prestressed Retrofit on Fatigue Life

The effect of the developed retrofit on resulting fatigue life is determined by comparing the fatigue performance of specimen C3-3 (having no retrofit) and C3-4 (having a retrofit and 13.65ksi prestress). Specimen C3-3 with no retrofit experienced fatigue cracking at the notch which resulted in complete cross-section fracture after 989,235 cycles. Considering a fatigue category E' detail, a notched weld, specimen C3-3 would be calculated to fail after 969,165 cycles which is fairly close to the experimental observation. Figure 25 shows the resulting fatigue fracture emanating from the induced notch. Application of the retrofit in specimen C3-4 increased the number of cycles to failure for the half-scale gate specimen to 2,911,198 cycles (a fatigue life increase of nearly 3 times over the un-retrofitted specimen). Figure 26 shows a comparison of the stress within the notch for the specimens C3-3 (un-retrofitted) and C3-4 (retrofitted), with the reduced notch stress resulting in increased fatigue life. In Figure 26, application of the retrofit

initially decreased the notch stress by 20.5ksi as compared to the unretrofitted specimen C3-3. Note however that the retrofit did not perform as well as intended, due to a prestress loss that was observed at 50,000 cycles which resulted in an increase in notch stress (see Figure 26). This prestress loss was due to a debonding failure between the friction clamps and half-scale specimen and was corrected at 1,000,000 cycles during testing but eventually was lost again at 1,690,000 cycles. This prestress loss will be discussed further in the following section; however, it should be noted that even with prestress losses, the CFRP continued to take load resulting in a reduced notch stress of nearly 4.8 ksi (see Figure 26).

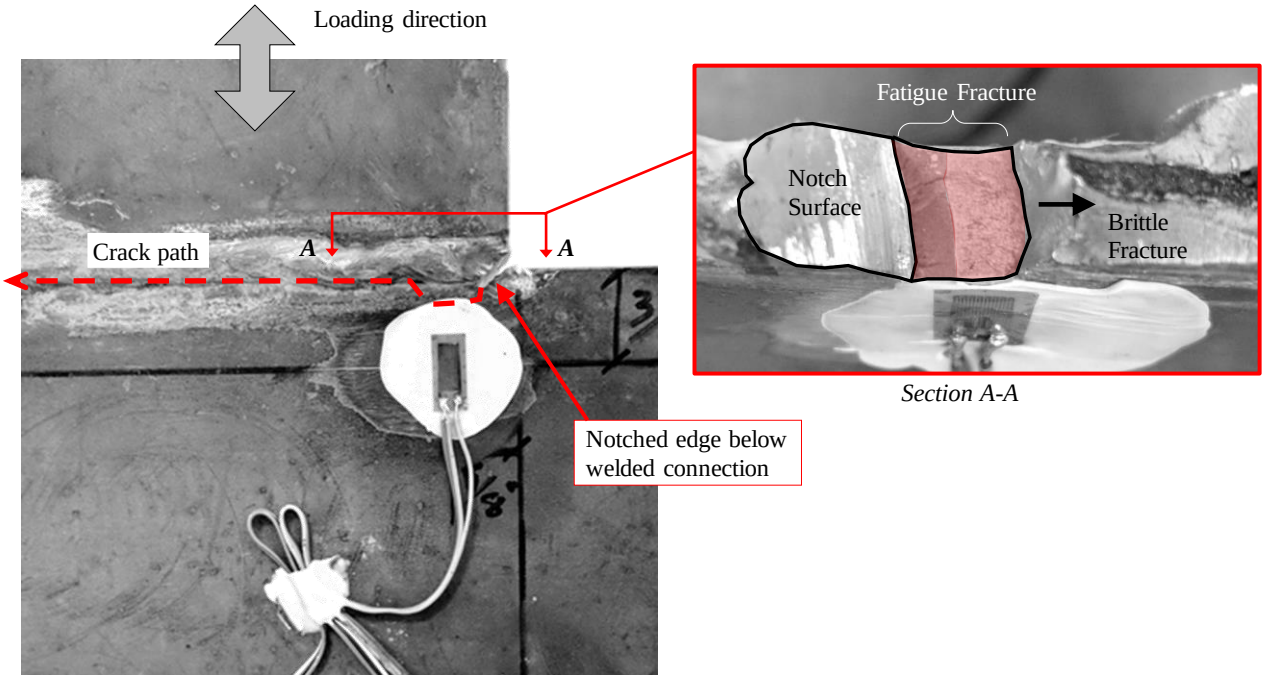

Figure 25. Fatigue fracture at the notch of specimen C3-3 following 989,235 cycles.

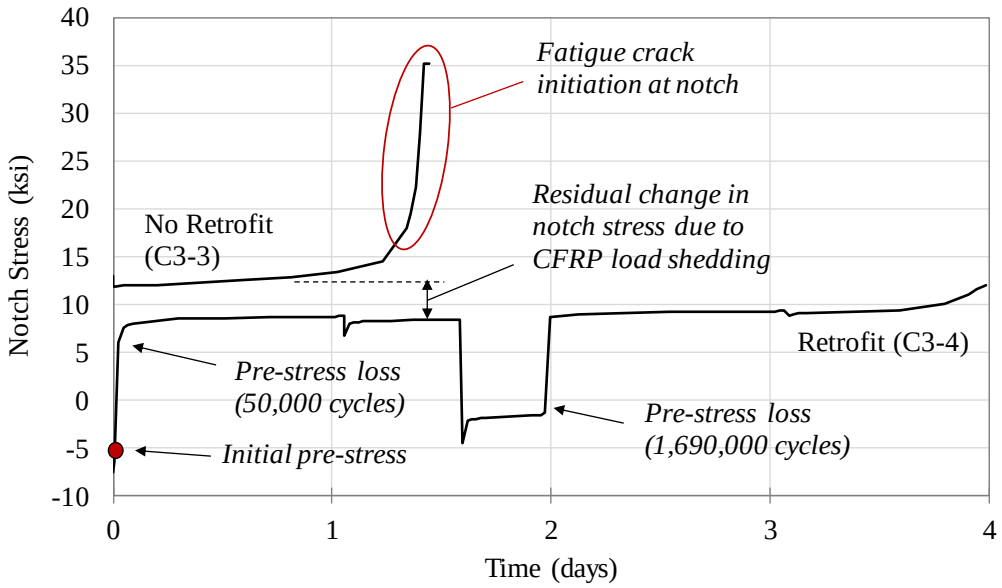

Figure 26. Measured stress at the notch of specimen C3-3 (no retrofit) and specimen C3-4 (retrofit)

4.5.4. Performance of Half-Scale Retrofit Clamping Mechanisms during Cyclic Loading

While the static retrofit bonding experiments were promising for inducing CFRP prestress levels up to 50ksi, vibrations during rapid cyclic loading ultimately affected the retrofit bond and resulting CFRP prestress within the retrofit system. Epoxy debonding between the retrofit and gate specimen was observed in each high-cycle fatigue test. As an example, Figure 27 shows the CFRP prestress levels during the half-scale test C3-4 (discussed previously), where the initial prestress of 13.7ksi was reduced by 11.8ksi following approximately 50,000 cycles at 20Hz (41 minutes of loading) due to debonding of the retrofit clamps from the specimen surface. Following 1,000,000 cycles, an additional prestress was performed to 10.15ksi by allowing the debonded retrofit clamp to bear on the specimen weld profile, which resulted in the other retrofit clamp to debond after an additional 690,000 cycles (9 hours and 35 minutes of testing in Figure 27). Note that even though the retrofit clamps debonded, the CFRP material continued to take some of the applied axial load (equal to the applied clamping friction force). Given the results of the epoxy

performance during fatigue loading, future retrofit performance may be improved by using the SlipnotTM surface which had similar static prestress results but relies on friction over adhesion to maintain CFRP prestress levels.

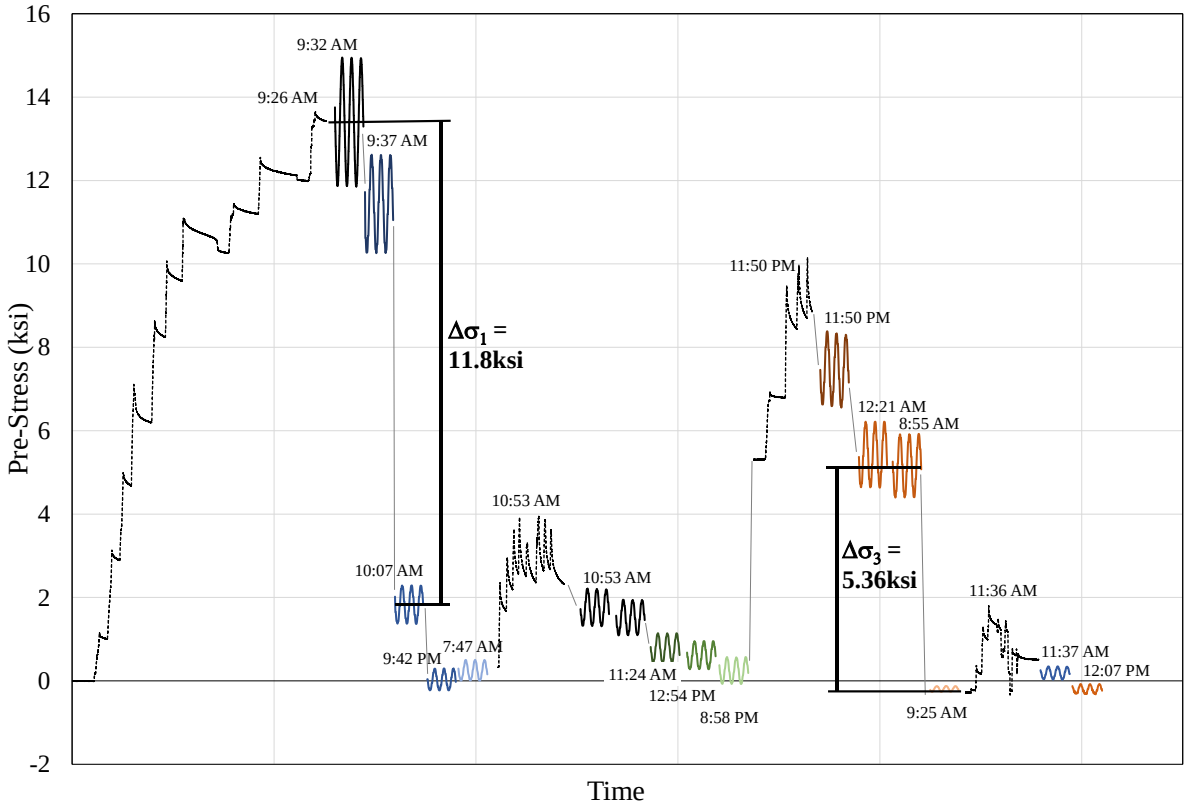

Figure 27. Measured CFRP prestress during rapid cyclic loading.

5. Summary and Conclusions

In this study, a prestressed CFRP retrofit was developed for controlling local stress states within lock gate structures. The study retrofit development involved CFRP prestressing strategies, bonding mechanisms, long-term prestress performance and large-scale experimental fatigue testing. In addition to various bonding experiments, a total of seven large-scale cyclic tests were conducted on lock gate components (with and without applied retrofits) to gauge the effectiveness

of the developed prestressing strategies. The following conclusions were found from the experimental testing:

- Application of the prestressed retrofit on the notched half-scale specimen increased the fatigue life by more than 1.9 million cycles (a fatigue life increase of nearly 3 times over the un-retrofitted specimen).
- Prestressing strategies considering friction alone can achieve CFRP prestress levels similar to those with epoxy adhesives. The Slipnot^{TM} high friction coating and epoxy bonded CFRP both achieved similar prestress levels prior to slip at slightly more than 50ksi of CFRP prestress.
- Creep and relaxation within the prestressing system contributed to minor prestress losses. The full-scale epoxy-bonded CFRP specimen converged to approximately 10% prestress loss after 14 days.
- The applied CFRP prestress is capable of reducing the local stress felt at the notch of both the full-scale and half-scale specimens; however, prestress loss did occur due to epoxy adhesive debonding during rapid cyclic loading.
- Load shedding into the CFRP, even without significant prestress applied, contributed to reductions in component notch stresses. Even after debonding, the applied CFRP clamping force was able to provide enough force transfer to the CFRP to reduce the notch local stresses (see again Figure 26).

6. References

[1] USACE (2014). "Lock characteristics general report," *US Army Corps of Engineers, Navigation Data Center*.

[2] ASCE (2013). "Report card for America's infrastructure," *American Society of Civil Engineers*.

[3] ASCE (2017). "Infrastructure report card," *American Society of Civil Engineers*.

[4] ASCE (2018), "What makes a grade?," *American Society of Civil Engineers*.

[5] D. V. Grier (2017), "The Declining Reliability of the U.S. Inland Waterway System," *Homeland Security Digital Library*.

[6] P. Glass. (2012). "Head Lock". *Work Boat*, Accessed July 2, 2018 from: https://www.workboat.com/archive/head-lock/

[7] The Navigation Economic Technologies Program (2005), "McAlpine Lock Closure in August 2004," *US Army Corps of Engineers*, IWR Report 05-NETS-R-08.

[8] J. Brinckman (2009), "Dam's lock closure hurts Northwest shippers but could have been far worse," in *The Oregonian*, Accessed June 13, 2018 from: https://www.oregonlive.com/business/index.ssf/2009/10/post_1.html

[9] B. Chapman (2010), "LRD's Lock Gate Replacement Program," in *Briefing to Inland Waterways User Board*, US Army Corps of Engineers.

[10] Federal Highway Administration (2013), "Manual for Repair and Retrofit of Fatigue Cracks in Steel Bridges," *US Department of Transportation*.

[11] R. Prince (2018), "Fiber Reinforced Polymers Characteristics and Behaviors," *Build on Prince*, Accessed June 15, 2018 from: https://www.build-on-prince.com/fiber-reinforced-polymers.html

[12] B. M. Phares, T. J. Wipf, F. W. Klaiber, A. Abu-Hawash, and Y.-S. Lee (2003), "Strengthening of steel girder bridges using FRP," presented at the Proc. 2003 Mid-Continent Transportation Research Symposium, Ames, IA Aug. 21-22.

[13] F. Matta, C. Aquino, A. Nanni, and J. Giancaspro (2007), "Unbonded CFRP Bar System for External Post-Tensioning," presented at the American Composites Manufacturers Association, Tampa, FL USA.

[14] M. Tavakkolizadeh and H. Saadatmanesh (2003), "Fatigue Strength of Steel Girders Strengthened with Carbon Fiber Reinforced Polymer Patch," *Journal of Structural Engineering*, vol. 129, pp. 186-196.

[15] P. P. Bansal, R. Sharma, and A. Mehta (2016), "Retrofitting of RC girders using prestressed CFRP sheets," *Steel and Composite Structures,* vol. 20, pp. 833-849.

[16] Y. Huawen, C. König, T. Ummenhofer, Q. Shizhong, and R. Plum (2010), "Fatigue Performance of Tension Steel Plates Strengthened with Prestressed CFRP Laminates," *Journal of Composites for Construction,* vol. 14, pp. 609-615.

[17] H. K. Nordin and B. R. Täljsten (2006), "Concrete Beams Strengthened with Prestressed Near Surface Mounted CFRP," *Journal of Composites for Construction,* vol. 10, pp. 60-68.

[18] B. R. Täljsten, C. S. Hansen, and J. W. Schmidt (2009), "Strengthening of old metallic structures in fatigue with prestressed and non-prestressed CFRP laminates," *Construction and Building Materials,* vol. 23, pp. 1665-1677.

[19] E. Ghafoori and M. Motavalli (2015), "Lateral-torsional buckling of steel I-beams retrofitted by bonded and un-bonded CFRP laminates with different prestress levels: Experimental and numerical study," *Construction and Building Materials,* vol. 76, pp. 194-206.

[20] A. Lenwari, T. Thepchatri, and P. Albrecht (2006), "Debonding Strength of Steel Beams Strengthened with CFRP Plates," *Journal of Composites for Construction,* vol. 10, pp. 69-78.

[21] P. Colombi, A. Bassetti, and A. Nussbaumer (2003), "Analysis of cracked steel members reinforced by prestress composite patch," *Fatigue & Fracture of Engineering Materials & Structures,* vol. 26, pp. 59-66.

[22] F. Kianmofrad, E. Ghafoori, M. M. Elyasi, M. Motavalli, and M. Rahimian (2017), "Strengthening of metallic beams with different types of prestressed un-bonded retrofit systems," *Composite Structures,* vol. 159, pp. 81-95.

[23] F. M. Mohee and A. Al-Mayah (2017), "Development of an innovative prestressing CFRP plate anchor: Numerical modelling and parametric study," *Composite Structures,* vol. 177, pp. 1-12.

[24] S. Hong and S.-K. Park (2017), "Concrete Beams Strengthened With Prestressed Unbonded Carbon-Fiber-Reinforced Polymer Plates: An Experimental Study," *Polymer Composites,* vol. 38, pp. 2459-2471.

[25] H. Ye, C. Li, S. Pei, T. Ummenhofer, and H. Qu (2018), "Fatigue Performance Analysis of Damaged Steel Beams Strengthened with Prestressed Unbonded CFRP Plates," *Journal of Bridge Engineering,* vol. 23, pp. 1-12.

[26] J. Li, Y. Wang, J. Deng, and Y. Jia (2018), "Experimental study on the flexural behavior of notched steel beams strengthened by prestressed CFRP plate with an end plate anchorage system," *Engineering Structures,* vol. 171, pp. 29-39.

[27] E. Ghafoori, M. Motavalli, A. Nussbaumer, A. Herwig, G. S. Prinz, and M. Fontana (2015), "Design criterion for fatigue strengthening of riveted beams in a 120-year-old railway metallic bridge using prestressed CFRP plates," *Composites: Part B,* vol. 68, pp. 1-13.

[28] E. Ghafoori, M. Motavalli, A. Nussbaumer, A. Herwig, G. S. Prinz, and M. Fontana (2016), "Fatigue strengthening of riveted girders in a historic railway metallic bridge in Switzerland using prestressed un-bonded CFRP laminates," *Proc. of the 8th Int. Conf. on Bridge Maintenance, Safety and Management,* pp. 1-8.

[29] C. M. Lozano (2017), "Development of Prestressed Retrofit Strategies for Mitigating Fatigue Cracking in Steel Waterway Lock Gate Components," *M.S. Thesis,* University of Arkansas, Fayetteville, AR.

[30] AASHTO (2012), "AASHTO LRFD bridge design specifications (6th edition)," *American Association of State Highway and Transportation Officials,* pp. Washington, DC.

[31] W. D. Pilkey (2005), "Stress Concentration," in *Formulas for Stress, Strain, and Structural Matrices*, ed: John Wiley & Sons, pp. 255-305.